

ab initio modeling of open systems: charge transfer, electron conduction, and molecular switching of a C_{60} device

Jeremy Taylor¹, Hong Guo¹, and Jian Wang²

1. Center for the Physics of Materials and Department of Physics, McGill University, Montreal, PQ, Canada H3A 2T8.
2. Department of Physics, The University of Hong Kong, Pokfulam Road, Hong Kong, China.

We present an *ab initio* analysis of electron conduction through a C_{60} molecular device. Charge transfer from the device electrodes to the molecular region is found to play a crucial role in aligning the lowest unoccupied molecular orbital (LUMO) of the C_{60} to the Fermi level of the electrodes. This alignment induces a substantial device conductance of $\sim 2.2 \times (2e^2/h)$. A gate potential can inhibit charge transfer and introduce a conductance gap near E_F , changing the current-voltage characteristics from metallic to semi-conducting, thereby producing a field effect molecular current switch.

72.80.Rj,73.61.Wp,73.23.Ad

Understanding electron conduction in atomic and molecular scale nano-devices is an extremely active research topic at present. In several recent experiments¹⁻⁶, electric current flowing through truly atomic and molecular scale conductors, as small as a single atom, have been measured. The current voltage (I-V) characteristics of these molecular devices have profound potential for device application, including high nonlinearity, negative differential resistance, and electro-mechanic current switching. However, a thorough understanding of electron transport mechanisms at this scale, which will play a crucial role in designing operation principles for future nanoelectronics, has not yet been achieved. To provide insight into electron conduction mechanisms at the atomic and molecular scale, we have investigated the quantum transport properties of a C_{60} based molecular device using a first principles theoretical method.

Experimentally, the C_{60} molecular electro-mechanical amplifier¹ demonstrated that electric current flowing through a C_{60} molecule could be amplified by as large as 100 times when the molecule was *mechanically* deformed. This phenomenon was attributed to an increase of the tunneling density of states at the Fermi level induced by the mechanical deformation^{1,7}. While this conduction mechanism is very interesting, a natural question is whether or not there are other, perhaps simpler, physical mechanisms which can be exploited for molecular scale electron conduction? Our analysis suggests a unique and new conduction mechanism based on charge transfer doping (CTD): because of its high electro-negativity, a well contacted C_{60} gains charge from CTD thereby aligning its LUMO state to the Fermi level of the electrodes resulting in a substantial device conductance without the need of mechanical deformation. CTD was seen to have

reduced the conductance of a short carbon chain⁸, but for the more complex C_{60} molecule, it does the opposite by drastically *increasing* conduction. Current switching mechanisms are another important yet unsettled question of nanoelectronics. Our analysis further suggests a new principle for molecular switching: using proper electro-negative molecules and metallic electrodes, current can be switched on and off by controlling the amount of charge that is transferred to the molecular region.

The C_{60} device we study is illustrated schematically in Fig.(1a) where a C_{60} molecule is electrically *well* contacted by two atomic scale Al metallic electrodes which extend to reservoirs far away where bias voltages $V_{l,r}$ are applied to the left (*l*) and right (*r*) electrodes, respectively. An additional gate voltage V_g may also be applied to a metallic gate capacitively coupled to the molecule. Due to the large number of atoms and complications such as the gate, the bias, the atomic electrodes (as opposed to jellium electrodes), and the presence of localized states, existing *ab initio* methods for analyzing quantum transport⁹⁻¹¹ cannot be applied. We have therefore developed a new approach which combines non-equilibrium Green's function theory^{12,13} with pseudo-potential real space *ab initio* simulation techniques¹⁴. It is worth noting that conventional density functional theory (DFT) methods solve problems for either finite systems such as an isolated molecule, or periodic systems consisting of super-cells. In contrast, central to our problem of predicting quantum transport properties is the ability to deal with systems having *open* boundaries provided by long electrodes which maintain different chemical potential due to external bias. In other words, a typical device geometry, *e.g.* Fig.(1a), is neither isolated nor periodic. This situation is most conveniently handled by nonequilibrium Green's function theory^{12,13}.

Briefly, our technique is outlined as follows¹⁵. We divide the long device system into three regions¹⁰: the left and right electrodes, and the scattering region (Fig.(1a)). The scattering region actually includes a portion of the semi-infinite electrodes¹⁰. After self-consistency is reached, this arrangement ensures good electric contact between the electrodes and the molecule, establishes a common Fermi level for the system, and ensures charge neutrality at equilibrium. When the scattering region is large enough^{10,16}, the Kohn-Sham (KS) potential outside the scattering region is well screened and therefore well approximated by a perfect "bulk" electrode environment which we obtain by a separate calculation¹⁶. By setting the KS potential outside the scattering region to

the bulk value and matching the electrostatic potential at the boundary (including the gate), the *infinite* open boundary problem is reduced to the calculation of charge density inside the *finite* scattering region with the electrodes' contribution accounted for by appropriate self-energies^{12,13,17}.

To perform our self-consistent DFT analysis, we calculate the charge density from the density matrix which is related to nonequilibrium Green's function^{12,13,17} operator,

$$\hat{\rho} = i \int_{-\infty}^{\infty} dE \mathbf{G}^<(E) = i \int_{-\infty}^{\infty} dE \mathbf{G}^R \Sigma^< \mathbf{G}^A \quad (1)$$

where^{12,13,17}:

$$\Sigma^< = \begin{bmatrix} f_l(E; \mu_l) \Sigma_{l,l}^E & 0 & 0 \\ 0 & 0 & 0 \\ 0 & 0 & f_r(E; \mu_r) \Sigma_{r,r}^E \end{bmatrix} \quad (2)$$

and $f_{l,r}(E; \mu_{l,r})$ are the distribution functions deep in the left and right electrodes with chemical potentials $\mu_{l,r}$, respectively. The reservoirs are assumed to be at equilibrium, therefore $f_{l,r} \approx \Theta(E - \mu_{l,r})$ at low temperatures where Θ is the step function. The retarded (and advanced) Green's functions \mathbf{G}^R (\mathbf{G}^A) of the system are then calculated in standard fashion¹⁷⁻¹⁹ by direct matrix inversion where self-energies due to coupling to electrodes ($\Sigma_{l,l}^E, \Sigma_{r,r}^E$) are calculated by extending the method of Ref. 18. Because there are many bands in our atomic electrodes (as compared to jellium electrodes^{9,10}), the energy integration of Eq. (1) must be done with care so that global charge neutrality is maintained at equilibrium. With the charge density, we can evaluate the effective device potential $V_{\text{eff}}[\rho(\mathbf{r})]$ which consists of Hartree, exchange-correlation, atomic core, and any other external potentials¹⁵. Using the boundary condition on the effective potential discussed above, $V_{\text{eff}}(\mathbf{r})$ is defined everywhere in space. It is therefore straightforward to construct the Hamiltonian matrix using an s, p Fireball atomic orbital basis set¹⁴. We use standard norm-conserving pseudopotentials to describe the atomic cores²⁰. The DFT iteration is repeated until self-consistency, and current is calculated by integrating conductance $G(E)$ over energy^{12,13,17}, with $G(E) = 4G_o \text{Tr}[Im(\Sigma_{ll}^E) \mathbf{G}^R Im(\Sigma_{rr}^E) \mathbf{G}^A]$ where $G_o = \frac{2e^2}{h}$.

Fig.(1b) shows the equilibrium charge distribution along the middle cross-section of the device²¹ at zero bias and gate voltages. The charge density in the electrodes is affected by the C_{60} but this effect is well screened away from the molecule. Indeed, the charge density contours match perfectly at the connections between the electrodes and the scattering region²¹. The electronic structure of an isolated C_{60} molecule is well known²² and our *ab initio* calculation gives a HOMO-LUMO gap of 1.77eV, in excellent agreement with previous literature²³. The undoped C_{60} *molecular solid* is a semiconductor²². Since C_{60} is electro-negative, one can dope the solid and

fill the LUMO state with up to 6 electrons²². Importantly, for our device the *open* metallic electrodes provide natural doping through CTD. As a result, we found that, in equilibrium, three extra electrons flow into the molecular region. This is a substantial charge transfer in order for the molecule to equilibrate with the electrodes so that a common Fermi level is established. Experimentally, it is found that the C_{60} solid conducts best when it is doped with three electrons per C_{60} ²². This is because doping three electrons amounts to half filling the LUMO. Our *ab initio* analysis predicts, for the C_{60} device, that the C_{60} LUMO state is half-filled and we find an equilibrium conductance of $G(E_F) = 2.2G_o$ at zero temperature. This value is very significant: without charge transfer we would expect a much smaller conductance due to the filled HOMO state and the substantial HOMO-LUMO gap of the isolated C_{60} .

In Fig.(2), we plot the equilibrium transmission eigenvalues of the device as a function of electron energy at two different gate voltages. At $V_g = 0$, there are three transmission eigenvectors which contribute substantially at E_F (the vertical line) to the equilibrium conductance $G = 2.2G_o$. However, a gate voltage shifts the states near E_F and changes the transmission channels significantly. This is shown in Fig.(2b) where we see a conductance gap at E_F . Therefore, a gate potential can change electron conduction through this device significantly, producing field induced molecular switching. We can understand the transport properties by projecting the scattering states of the device on to the molecular orbitals of an isolated C_{60} . We found that scattering states near E_F are over 90% HOMO or LUMO in character, indicating that the C_{60} retains its isolated electronic structure and that other C_{60} orbitals are less important for conduction. In addition, we can classify each scattering state as being majority HOMO or majority LUMO. We find that majority HOMO states are almost pure HOMO (> 90%); while majority LUMO states are a HOMO-LUMO mixture (~30:70). Specifically, the transmission eigenvectors of Fig.(2a) are all LUMO-like, indicating that there are three electrons half filling the LUMO state and contributing three conduction channels at equilibrium. In other words, the LUMO state is naturally aligned with E_F due to charge transfer. On the other hand, a negative gate voltage can inhibit charge transfer so that E_F lies between the HOMO and LUMO states of the molecule. Indeed, we found that the scattering state corresponding to the left peak in Fig.(2b) is HOMO-like, and that of the right peak is LUMO-like. In the absence of charge transfer, one would expect transmission properties similar to those in Fig. (2b).

The above physical picture is further demonstrated in Fig. (3) which shows the equilibrium conductance G , the three individual transmission eigenvalues T_i ($i = 1, 2, 3$), and the number of transferred charge Q (inset) as functions of gate voltage V_g at E_F . G has a step-like behavior: each "step" is due to the depletion of a LUMO-like state. Only after charge transfer is completely inhibited

do we obtain the conductance gap illustrated in Fig.(2b) where G becomes very small. Our result therefore indicates that charge transfer plays a crucial role and changes the physical picture of electron conduction in this device qualitatively. The behavior of G also has a clear correspondence with T_i (the dotted lines with circles): as V_g is scanned toward more negative values, T_i 's are removed one by one.

Charge transfer also has very important implications for the I-V curves, shown in Fig.(4). The current is plotted as a function of right bias V_r , fixing $V_l = 0$. When $V_g = 0$ the I-V curve shows clear metallic behavior. When $V_g \neq 0$, the C_{60} device can change from a metal (Fig. (2a)) to a semiconductor (Fig. (2b)) with a conductance gap near zero bias. Therefore the gate potential can "switch" off the current, reflecting the transition of transmission eigenvalues from Fig.(2a) to (2b). This corresponds to an amplification factor of ~ 20 . The value of gate potential is non-universal as it depends on the shape of the gate and dielectric medium surrounding the device. What is essential is to produce enough electric field lines inside the molecular region so that the electrode-doped LUMO electrons are depleted from the molecular junction. For our system, a shift of $\sim 0.1\text{eV}$ is enough to generate switching. This is however a large shift and it suggests that a sharp-shaped gate is perhaps necessary in an experimental setup, otherwise most field lines will be screened by the metallic electrodes. The predicted current is in the range of $\sim 10\mu\text{A}$ at small bias voltages ($\sim 50\text{mV}$). This is somewhat larger than the $\sim 4\mu\text{A}$ measured for the electro-mechanic amplifier^{1,24}.

Our results also have important implications and provide a benchmark for semi-empirical and other theories, such as those based on parameterized tight binding models. The chemical potential difference between an isolated Al electrode and an isolated C_{60} molecule is $\Delta \equiv E_F^{\text{electrode}} - E_F^{C_{60}} \sim 0.19a.u.$. This provides a lot of uncertainty as how one should align the molecular orbitals to the Fermi level of the electrodes in a non-self-consistent calculation. Specifically²⁵, calculating $G(E_F^{\text{electrode}})$ without alignment gives $1.17G_o$, much less than the correct result. Shifting levels of C_{60} by adjusting a chemical potential so that global charge neutrality is obtained, we get $1.7G_o$. Shifting levels so that three extra charges are inside C_{60} region, the result becomes $2.0G_o$. Because we cannot know charge transfer in a non-self consistent analysis, the result suggests that requiring global charge neutrality in a semi-empirical calculation is the next best thing to do at equilibrium. In this regard, we note that there has been some practice for requiring local charge neutrality on each atom^{26,27} in semi-empirical calculations. Another interesting result we found is that there are many localized states in the molecular junction. At equilibrium, we find 96 bound states by integrating the density of states (Eq.(1)) from $-\infty$ to the propagating threshold of the electrodes. These localized states play an important role in establishing the effective potential V_{eff} and must be included

in the analysis.

In summary, our results suggest that charge transfer doping induces a substantial conductance in a well contacted molecular C_{60} device. Essentially, CTD aligns the LUMO states of the C_{60} with the Fermi level of the electrodes, opening up 3 conductance channels and producing metallic I-V characteristics at equilibrium. A field effect provided by a gate potential can switch off the current by inhibiting charge transfer. This is very interesting from a device operation point of view and provides a new mechanism for molecular scale current switches, complementing the electro-mechanical operation principle explored in previous work¹. The charge transfer induced conduction discussed here should be a more general mechanism: using proper electrodes which provide natural doping to electro-negative molecular systems with a filled HOMO state and substantial HOMO-LUMO gap, an increase in conduction is expected. Since one expects charge transfer to be a generic feature of molecular devices, this effect should be exploited further for applications of molecular scale current switches.

Acknowledgments: We gratefully acknowledge financial support from NSERC of Canada and FCAR of Quebec (H.G); RGC grant (HKU 7215/99P) from the Hong Kong SAR (J.W.). J.T gratefully acknowledge financial support from NSERC through a PG Fellowship.

-
- ¹ C. Joachim, J.K. Gimzewski, R.R. Schlittler, and C. Chavy, Phys. Rev. Lett. **74**, 2102 (1995); J.K. Gimzewski and C. Joachim, Science, **283**, 1683 (1999).
 - ² A. Yazdani, D.M. Eigler and N. Lang, Science, **272**, 1921 (1996).
 - ³ S.J. Tans, *et.al.* Nature 386, 474 (1997).
 - ⁴ J.W.G. Wildoer, *et.al.*, Nature, **393**, 49 (1998); D. Porath, A. Bezryadin, S. de Vries and C. Dekker, Nature, **403**, 635 (2000).
 - ⁵ M.A. Reed, *et.al.*, Science, **278**, 252 (1997); J. Chen, M.A. Reed, A.M. Rawlett, J.M. Tour, Science, **286**, 1550 (1999).
 - ⁶ Y. Xue, *et.al.*, Phys. Rev. B. **59**, R7852 (1999).
 - ⁷ C. Joachim, J.K. Gimzewski and H. Tang, Phys. Rev. B. **58**, 16407 (1998).
 - ⁸ N.D. Lang and Ph. Avouris, Phys. Rev. Lett. **84**, 358 (2000).
 - ⁹ N.D. Lang, Phys. Rev. B. **52**, 5335 (1995); M. Di Ventra, S.T. Pantelides and N.D. Lang, Phys. Rev. Lett. **84**, 979 (2000).
 - ¹⁰ C.C. Wan, J.L. Mozos, G. Tarachi, J. Wang and H. Guo, Appl. Phys. Lett., **71**, 419 (1997); J. Wang *et.al.*, Phys. Rev. Lett., **80**, 4277 (1998); G. Taraschi *et.al.*, Phys. Rev. B **58**, 13138 (1998); J.L. Mozos, *et.al.*, Phys. Rev. B **56**, R4351 (1997).
 - ¹¹ H.J. Choi and J. Ihm, Phys. Rev. B 59, 2267 (1999).
 - ¹² A. P. Jauho, N. S. Wingreen, and Y. Meir, Phys. Rev. B **50**, 5528 (1994).

- ¹³ B.G. Wang, J. Wang and Hong Guo, Phys. Rev. Lett. **82**, 398 (1999); J. Appl. Phys., **86**, 5094(1999).
- ¹⁴ P. Ordejón, E. Artacho and José M. Soler, Phys. Rev. B. **53**, R10441 (1996).
- ¹⁵ The detailed numerical procedure will be published elsewhere, J. Taylor and H. Guo, unpublished.
- ¹⁶ J. Wang, Y.J. Wang, and H. Guo, J. Appl. Phys. **75**, 2721(1994); Y.J. Wang, J. Wang, H. Guo and E. Zaremba, Phys. Rev. B **52**, 2738 (1995).
- ¹⁷ S. Datta, *Electronic Transport in Mesoscopic Systems*, (Cambridge University Press, New York, 1995).
- ¹⁸ S. Sanvito, C.J. Lambert, J.H. Jefferson, A.M. Bratkovsky, Phys. Rev. B, **59**, 11936 (1999).
- ¹⁹ H. Mehrez, *et.al.*, Phys. Rev. Lett., **84**, 2682 (2000); C. Roland, M.Buongiorno Nardelli, Jian Wang and Hong Guo, Phys. Rev. Lett., **84**, 2921-2924 (2000).
- ²⁰ D.R. Hamann, M. Schlüter, and C. Chiang, Phys. Rev. Lett. **43**, 1494 (1982).
- ²¹ For simplicity we have fixed the atomic positions. The electrode-molecule distance is kept at 1.06Å for the results presented here. We have confirmed that there is no qualitative change to the results when this distance is varied so long as bonding between electrodes and the molecule exists. An Al electrode is represented by a slab of Al oriented along the (100) plane with eighteen atoms per unit cell. We have confirmed that doubling the electrode length (the portion included inside the scattering region) gives essentially the same result. The matching of the charge density contours (Fig.(1b)) gives a strong confirmation of the numerical accuracy as the boundary condition on the potential has generated a perfect match of the charge density.
- ²² *Science of Fullerenes and Carbon Nanotubes*, M.S. Dresselhaus, G. Dresselhaus and P.C. Eklund, (Academic Press Inc., New York, 1996).
- ²³ Average gap value from the literature is 1.8eV. See, for example, p458 of Ref. 22.
- ²⁴ We do not expect an exact agreement because of the different physical mechanisms for conduction. In addition, the C_{60} in our device is very well contacted which tends to give a larger current.
- ²⁵ We have carried out the non-self-consistent calculation using the Harris functional.
- ²⁶ P.L. Pernas, A. Martin-Rodero and F. Flores, Phys. Rev. B. **41**, R8553 (1990).
- ²⁷ M. Brandbyge, N. Kobayashi and M. Tsukada, Phys. Rev. B. **60**, 17064 (1999).

FIG. 1. (a). Schematic plot of the C_{60} molecular device. (b). Contour plot of the equilibrium charge density. Notice the perfect match across the boundaries between the scattering region and the electrodes.

FIG. 2. Transmission eigenvalues as a function of electron energy. (a) For $V_g = 0$ where there are three transmission eigenvalues. (b) For $V_g = 1$ a.u. Vertical line shows the Fermi level of the system.

FIG. 3. Solid squares: equilibrium conductance $G(E_F)$ as a function of gate voltage V_g . Vertical dotted lines indicate, approximately, integer number of transferred charges Q . Open circles: the three transmission eigenvalues as a function of V_g at E_F . Inset: the transferred charge as a function of gate voltage.

FIG. 4. I-V curves of the system showing the switching between metallic (squares) and “semiconducting” (circles) behavior.

fig. 1

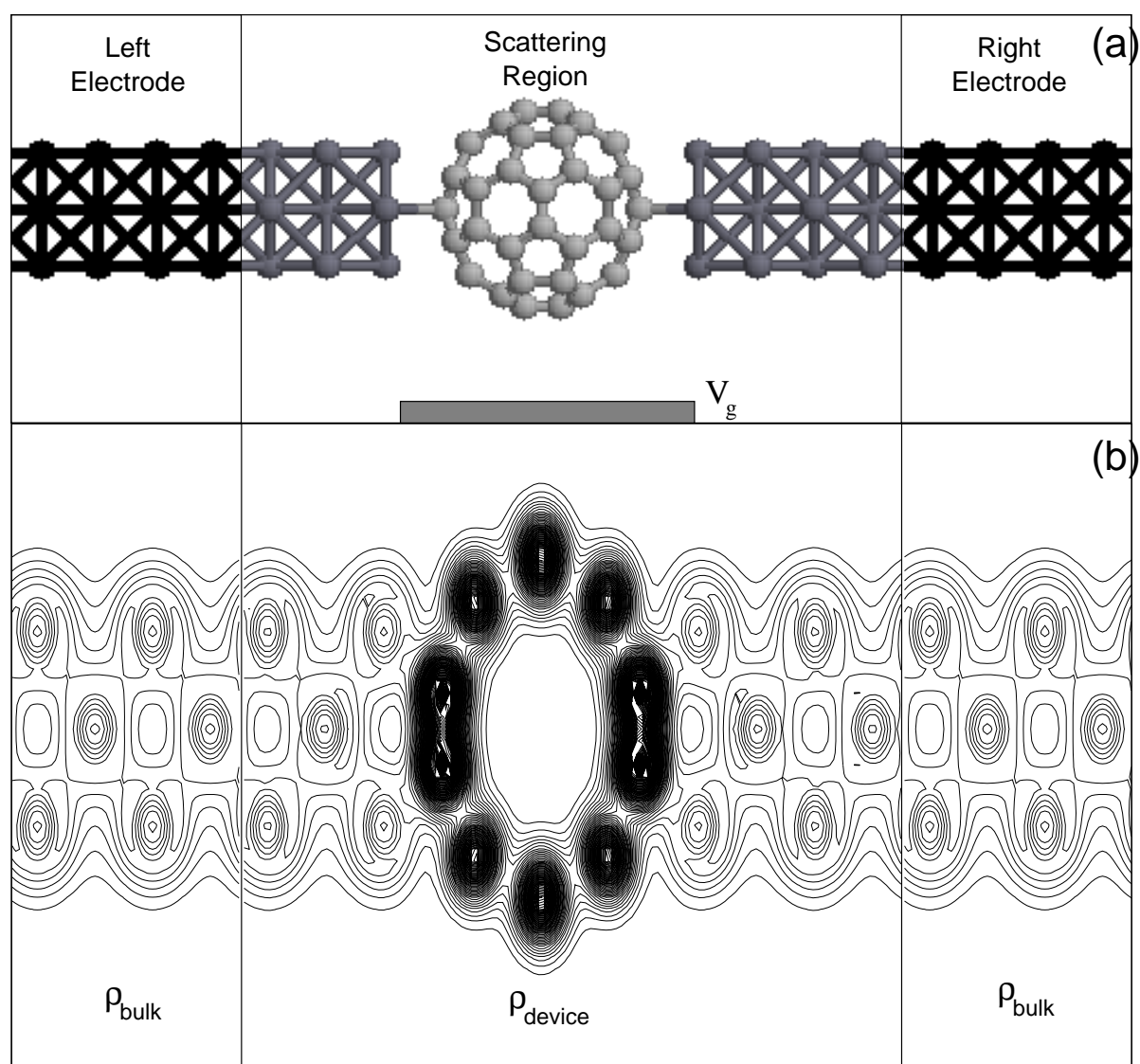


fig.2

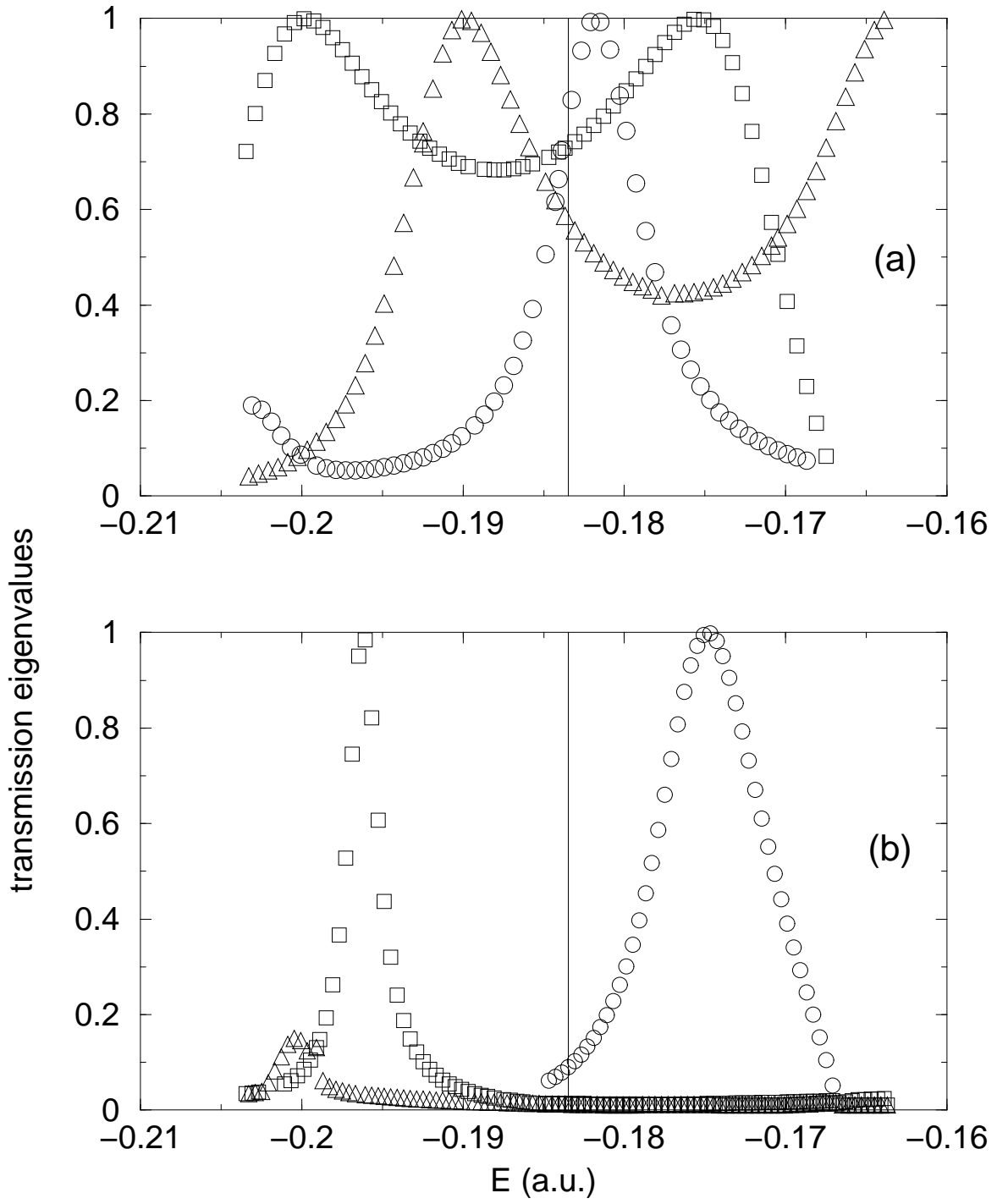


fig.(3)

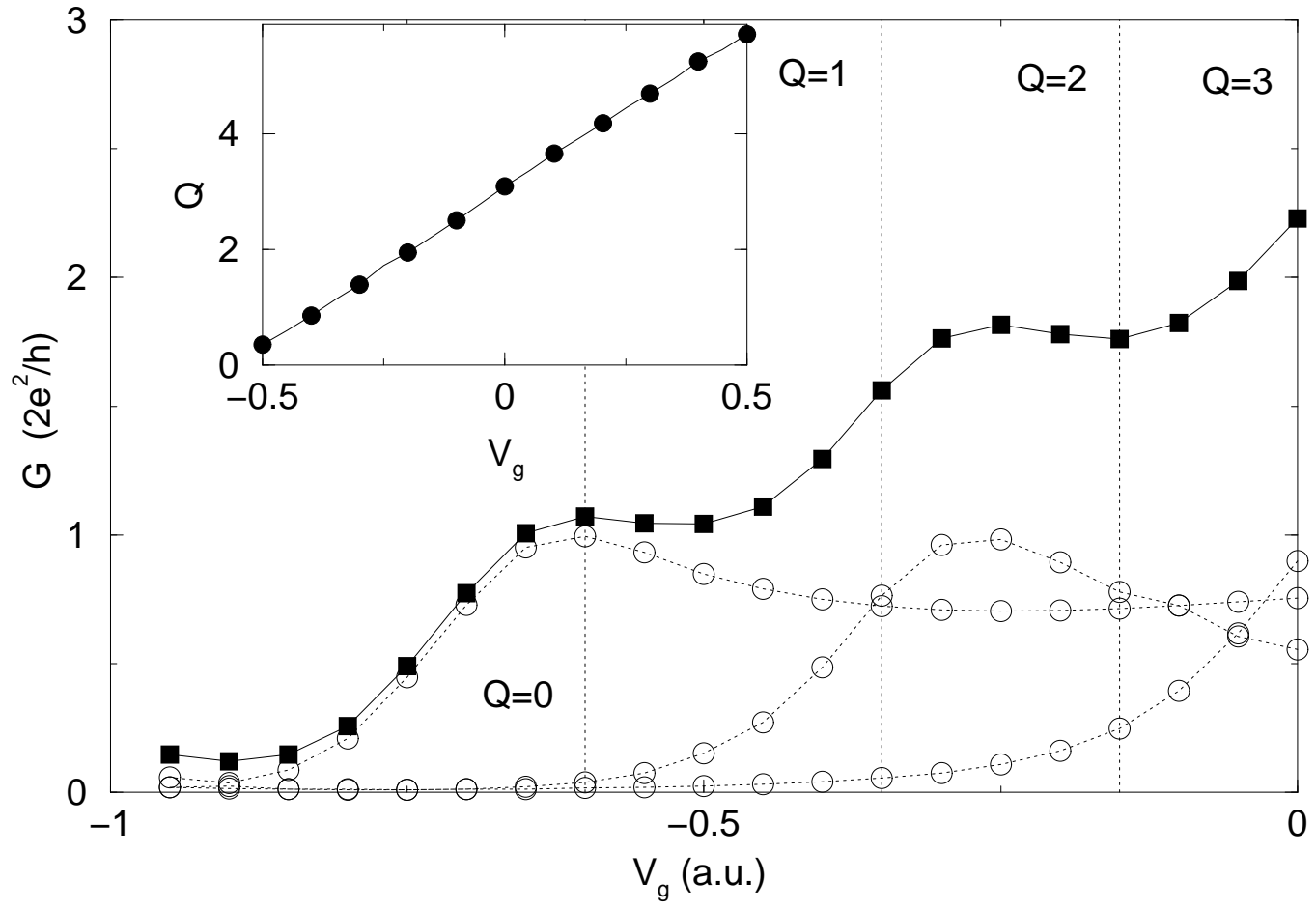


fig.(4)

